Hindawi
Mathematical Problems in Engineering
Volume 2021, Article ID 8817435, 16 pages
https://doi.org/10.1155/2021/8817435

Research Article

Magneto-Burgers Nanofluid Stratified Flow with Swimming Motile Microorganisms and Dual Variables Conductivity Configured by a Stretching Cylinder/Plate

Hassan Waqas,[1] Umair Manzoor,[1] Zahir Shah,[2] Muhammad Arif,[3] and Meshal Shutaywi[4]

[1]*Department of Mathematics, Government College University Faisalabad, Layyah Campus, Layyah 31200, Pakistan*
[2]*Department of Mathematics, University of Lakki Marwat, Lakki Marwat 28420, Khyber Pakhtunkhwa, Pakistan*
[3]*Department of Mathematics, Abdul Wali Khan University, Mardan 23200, Pakistan*
[4]*Department of Mathematics, College of Science & Arts, King Abdulaziz University, P.O. Box 344, Rabigh 21911, Saudi Arabia*

Correspondence should be addressed to Zahir Shah; zahir1987@yahoo.com

Received 29 September 2020; Revised 28 November 2020; Accepted 15 December 2020; Published 4 January 2021

Academic Editor: Ivan D. Rukhlenko

Background. The study of nanofluid gains interest of researchers because of its uses in treatment of cancer, wound treatment, fuel reserves, and elevating the particles in the bloodstream to a tumour. This artefact investigates the magnetohydrodynamic flow of Burgers nanofluid with the interaction of nonlinear thermal radiation, activation energy, and motile microorganisms across a stretching cylinder. *Method*. The developed partial differential equations (PDEs) are transformed into a structure of ODEs with the help of similarity transformation. The extracted problem is rectified numerically by using the bvp4c program in computational software MATLAB. The novelty of analysis lies in the fact that the impacts of bioconvection with magnetic effects on Burgers nanofluid are taken into account. Moreover, the behaviours of thermal conductivity and diffusivity are discussed in detail. The impacts of activation energy and motile microorganism are also explored. No work has been published yet in the literature survey according to the authors' knowledge. The current observation is the extension of Khan et al.'s work [51]. *Results*. The consequences of the relevant parameters, namely, thermophoresis parameter, Brownian motion parameter, the reaction parameter, temperature difference parameter, activation energy, bioconvection Lewis number and Peclet number against the velocity of Burgers nanofluid, temperature profile for nanoliquid, the concentration of nanoparticles, and microorganisms field, have been explored in depth. The reports had major impacts in the development of medications for the treatment of arterial diseases including atherosclerosis without any need for surgery, which may reduce spending on cardiovascular and postsurgical problems in patients. *Conclusions*. The current investigation depicts that fluid velocity increases for uplifting values of mixed convection parameter. Furthermore, it is analyzed that flow of fluid is risen by varying the amount of Burgers fluid parameter. The temperature distribution is escalated by escalating the values of temperature ratio parameter and thermal conductivity parameter. The concentration field turns down for elevated values of Lewis number and Brownian motion parameter, while conflicting circumstances are observed for the thermophoresis parameter and solutal Biot number. Larger values of Peclet number reduce the microorganism's field. Physically the current model is more significant in the field of applied mathematics. Furthermore, the current model is more helpful to improve the thermal conductivity of base fluids and heat transfer rate.

1. Introduction

Numerous scholars are fascinated by nanofluids due to their larger thermophysical properties and uses in heavy industrial and engineering technologies. Nanofluids contain fictional features that make them extremely useful and have gained substantial interest owing to their huge variety of applications such as cooling factors in electrical devices, automobiles, industrial-grade engines, and factories to improve efficiency, save energy, and minimize emission levels.

Nanofluids are also used as medicines and antibiotics in the biological sciences. Choi rendered the first use of nanofluid in 1995 [1]. Buongiorno [2] suggested two key features, thermophoresis and Brownian motion, to advance the convection of nanofluids. The hybrid nanofluids in the various kinds of heat structure for specific boundary constraints and physical scrutinized by Humic [3]. The two-dimensional Darcy-Forchheimer nanofluid flow over the curved stretching layer was analyzed by Hayat et al. [4]. Ellahi et al. [5] explored the role of the slip in the two-phase nanofluid flow. The analysis of mixed convection flow over a vertical sheet having hybrid nanoparticles with porous medium was observed by Waini et al. [6]. Ahmed et al. [7] addressed the entropy generation in magnetohydrodynamics Eyring–Powell nanoliquids flow with the consequences of dissipation, nonlinear mixed convection, and Joule heating. Lahmar et al. [8] reported the flow and heat transfer of a squeezing unsteady nanofluid between two parallel plates. First and second law study of aqueous (NF) including suspended Ag nanoadditives in two new microchannel heat sinks is analyzed by Yang et al. [9]. The steady nanofluid flow over a permeable stretch/shrink cylinder was evaluated by Roşca et al. [10]. Khan et al. [11] explored the behaviour of magnetic dipole on non-Newtonian fluid including nanoparticles. Abbas et al. [12] analyzed the characteristics of thermal conductivity on magnetized Carreau nanofluid. Abbas et al. [13] analyzed Wu's slip impacts on the magnetohydrodynamic flow of nanofluid with activation energy. Abbas et al. [14] discussed the thermal dependent viscosity on nanofluid with entropy generation. Abbas et al. [15] scrutinized the micropolar nanofluid with magnetic field under three-dimensional flows. There are many investigators who investigated the nanofluid behaviours [16–20].

The theory of heat and mass transfer in magnetohydrodynamic flow has many applications in a wide range of industrial applications, including geophysics, magnetic material processing, crude oil purification, and cooling rate control. The behaviour of energy equations under the Joule heating effect was discussed by Khan et al. [21]. The unstable flow of viscous fluid via magnetohydrodynamics was scrutinized by Ghalib et al. [22]. Khan et al. [23] premeditated 2-dimensional flow over a stretched surface of a non-Newtonian liquid with entropy optimization. Mohamad et al. [24] studied mixed convection of unstable noncoaxial viscous fluid rotational flow past an accelerated vertical disk. The effect of binary chemical reactions and activation energy on 3rd-grade hydromagnetic nanofluid streams combined with convective boundary layers was evaluated by Hayat et al. [25]. Iskender et al. [26] analyzed the steady flow of nanomaterials with melting heat phenomenon. Khedr et al. [27] explored the micropolar fluid with the impact of the magnetic field and heat source sink. Zaraki et al. [28] discussed the analysis of heat and mass transfer on nanomaterials liquid. Chamkha [29] analyzed the MHD flow under a porous medium over a vertical plate. Chamkha and Khaled [30] explored the coupled thermal and mass transfer over a permeable surface. Reddy et al. [31] scrutinized the heat and solutal transfer in nanofluid past a disk embedded in a porous medium. Many researchers [32–35] discussed the nanofluid properties over a different surface.

Bioconvection induced by variations in density of motile microorganisms is efficiently coordinated in the fields of ecological classifications, biogas, and production. The existence of such microorganisms improves the main density of the liquid and produces a gradient of density by floating that contributes to bioconvection. This fascinating discovery ultimately leads to an unstable, low-density layer. For example, microorganisms are spontaneously driven and move in the liquids to the atmosphere, while nanoparticles are directed by thermophoresis and Brownian motion in the surface liquid. Adding motile microorganisms to dilute nanomaterials suspensions is tremendously helpful for improving mass transport. Microorganisms were usually categorized as gyrotactic and gravitational microorganisms based on the pulsating force of different forms. There are still some different and related properties of nanostructures and motile microorganisms. The bioconvective stagnation point movement of nanoliquid, like swimming microorganisms, through a nonlinear stretching surface, is viewed by Mondal and Pal [36]. The Carreau-Yasuda nanofluid bioconvection flow in the appearance of microorganisms has been reported by Waqas et al. [37]. Two-dimensional generalized second-grade nanoliquid flow pasta Riga plate is investigated by Waqas et al. [38]. Khan et al. [39] analyzed the rheology of nanofluid stress couples using activation energy, thermal radiation, porous material, and convective boundary conditions of the field. The magnetized bioconvection movement of a nanofluid with microorganisms across a nonlinear inclined stretch sheet is intentional by Beg et al. [40]. Bhatti and Michaelides [41] inspect the activation energy of Arrhenius via the Riga plate for nanofluid thermobioconvection. Zadeh et al. [42] digitally observe the movement, heat, and mass transfer of nanofluids through a vertical stretch layer under the effect of motile microorganisms. Many researchers scrutinize the bioconvection aspects with nanofluids [43–48].

The main aspiration of the current inquiry is to evaluate the MHD flow of Burgers nanofluid configured by a stretching cylinder/plate. The consequences of thermal radiation, motile microorganisms, and chemical reactions are also taken into account. The governing equations of the flow problem are reduced by eminent shooting technique and cracked numerically with the bvp4c method via MATLAB commercial software. The effects of prominent parameters of the flow equation against velocity concentration and temperature profile are extracted numerically and graphically through graphs and tables. The considered problem may be helpful in industrial sectors. The current model is more useful in the field of technology to improve the heat transfer rate of heat storage devices. The proposed model is useful in automobiles, industrial-grid engines, cancer treatment, medicine, biosciences, biotechnology, pharmaceutical science, mechanical engineering, nuclear reactor, cooling of devices, and electrical engineering, as well as in many more fields. Bioconvectional model is more faithful in the biosensors, oil refineries, drugs delivery, medicines, chemotherapy, and military sectors.

2. Mathematical Formulation

In this article, we analyzed the consequences of Burgers nanofluid with the impacts of thermal radiation and motile microorganisms past a stretching cylinder/plate. Burgers nanofluid flow model over an expanding cylinder/plate is constructed with the strength of uniform magnetic field $B = [B_0, 0, 0]$ which is vertical to the flow path. Also, the temperature and concentration at the surface of the cylinder are supposed to be (T_w, C_w) each (see Figure 1).

$$\frac{\partial u}{\partial r}+\frac{u}{r}+\frac{\partial w}{\partial z}=0, \tag{1}$$

$$\begin{aligned}
&u\frac{\partial w}{\partial u}+w\frac{\partial w}{\partial z}+\beta_1\left[u^2\frac{\partial^2 w}{\partial r^2}+w^2\frac{\partial^2 w}{\partial z^2}+2uw\frac{\partial^2 w}{\partial z\,\partial r}\right]\\
&+\beta_2\left[\begin{array}{c}
u^3\dfrac{\partial^3 w}{\partial r^3}+w^3\dfrac{\partial^3 w}{\partial z^3}+2u^2\left(\dfrac{\partial u}{\partial r}\dfrac{\partial^2 w}{\partial r^2}+\dfrac{\partial w}{\partial r}\dfrac{\partial^2 w}{\partial r\,\partial z}\right)-u^2\left(\dfrac{\partial w}{\partial r}\dfrac{\partial^2 u}{\partial r^2}+\dfrac{\partial w}{\partial z}\dfrac{\partial^2 w}{\partial r^2}\right)\\
+2w^2\dfrac{\partial u}{\partial z}\dfrac{\partial^2 w}{\partial r\,\partial z}+w^2\left(\dfrac{\partial w}{\partial z}\dfrac{\partial^2 w}{\partial z^2}-\dfrac{\partial w}{\partial r}\dfrac{\partial^2 u}{\partial z^2}\right)+3uw\left(u\dfrac{\partial^3 w}{\partial r^2\partial z}+w\dfrac{\partial^3 w}{\partial z^2\partial r}\right)\\
+2uw\left(\dfrac{\partial u}{\partial r}\dfrac{\partial^2 w}{\partial z\,\partial r}+\dfrac{\partial u}{\partial z}\dfrac{\partial^2 w}{\partial r^2}+\dfrac{\partial w}{\partial r}\dfrac{\partial^2 w}{\partial z^2}-\dfrac{\partial w}{\partial r}\dfrac{\partial^2 u}{\partial r\,\partial z}\right)
\end{array}\right]\\
&=w_e\frac{\partial w_e}{\partial r}+\nu\beta_3\left[\begin{array}{c}
u^3\dfrac{\partial^3 w}{\partial r^3}+w\dfrac{\partial^3 w}{\partial r^2\partial z}+\dfrac{u}{r}\dfrac{\partial^2 w}{\partial r^2}-\dfrac{\partial w}{\partial r}\dfrac{\partial^2 u}{\partial r^2}+\dfrac{w}{r}\dfrac{\partial^2 w}{\partial r\,\partial z}\\
-\dfrac{1}{r}\dfrac{\partial u}{\partial r}\dfrac{\partial w}{\partial z}-\dfrac{1}{r}\dfrac{\partial w}{\partial r}\dfrac{\partial w}{\partial z}-\dfrac{\partial w}{\partial r}\dfrac{\partial u^2}{\partial z}
\end{array}\right]\\
&+\nu\left[\frac{\partial^2 w}{\partial r^2}+\frac{1}{r}\frac{\partial w}{\partial r}\right]-\frac{\sigma B_0^2}{\rho}\left[(w-w_e)\beta_1 u\frac{\partial w}{\partial r}+\beta_2\left(\begin{array}{c}
w\dfrac{\partial u}{\partial z}\dfrac{\partial^2 w}{\partial r^2}-u\dfrac{\partial w}{\partial z}\dfrac{\partial^2 w}{\partial r^2}\\
+uw\dfrac{\partial^2 w}{\partial r\,\partial z}+u^2\dfrac{\partial^2 w}{\partial r^2}
\end{array}\right)\right]\\
&+\frac{1}{\rho_f}\left[\begin{array}{c}
\left(1-C_f\right)\rho_f\beta^{**}g*(T-T_\infty)-\left(\rho_p-\rho_f\right)g^*(C-C_\infty)\\
-(N-N_\infty)g^*\gamma\left(\rho_m-\rho_f\right)
\end{array}\right]\sin\frac{\delta}{2},
\end{aligned} \tag{2}$$

$$u\frac{\partial T}{\partial r}+w\frac{\partial T}{\partial z}=\frac{1}{(\rho c)_f}\frac{\partial}{\partial r}\left[K(T)\frac{\partial T}{\partial r}\right]+\alpha_1\frac{1}{r}\left[\frac{\partial}{\partial r}\left(r\frac{\partial T}{\partial r}\right)\right]-\frac{1}{(\rho c)_f}\frac{\partial q_r}{\partial r}+\tau\left[D_b\frac{\partial D}{\partial r}\frac{\partial T}{\partial r}+\frac{D_T}{T_\infty}\left(\frac{\partial T}{\partial r}\right)^2\right], \tag{3}$$

$$u\frac{\partial C}{\partial r}+w\frac{\partial C}{\partial z}=\frac{\partial}{\partial r}\left[D(C)\frac{\partial C}{\partial r}\right]+\frac{D_B}{r}\frac{\partial}{\partial r}\left(r\frac{\partial C}{\partial r}\right)+\frac{D_T}{T_\infty}\frac{1}{r}\frac{\partial}{\partial r}\left(r\frac{\partial T}{\partial r}\right)-Kr^2(C-C_\infty)\left(\frac{T}{T_\infty}\right)^n\exp\left(\frac{-E_a}{kT}\right), \tag{4}$$

$$u\frac{\partial N}{\partial r}+w\frac{\partial N}{\partial z}+\left[\frac{\partial}{\partial r}\left(N\frac{\partial C}{\partial r}\right)\right]\frac{bW_c}{\left(C_f-C_\infty\right)}=D_m\frac{\partial}{\partial r}\left(\frac{\partial N}{\partial r}\right). \tag{5}$$

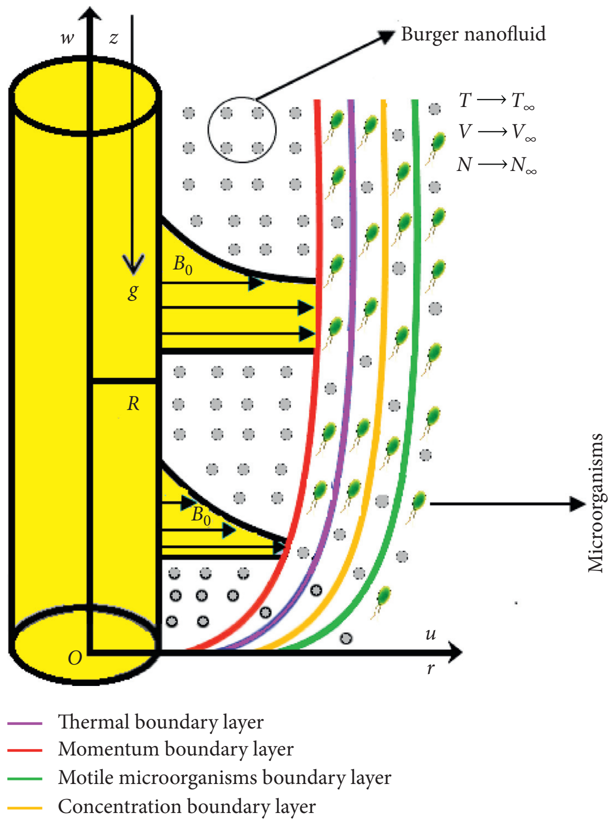

Figure 1: Physical view of flow.

In expressions (3) and (5), the thermal diffusivity and solutal diffusivity are read as $k(T)=k_\infty[1+\epsilon_1\ ((T-T_\infty)/(T_f-T_\infty))]$ and $D(C)=D_\infty[1+\epsilon_2\ ((C-C_\infty)/\ (C_f-C_\infty))]$. With boundary conditions

$$
\begin{aligned}
w &= w_S = \frac{U_0 z}{l},\\
u &= 0,\\
-k\frac{\partial T}{\partial r} &= h_f\left(T_f - T\right),\\
-D_B\frac{\partial C}{\partial r} &= h_g\left(C_f - C\right),\\
-D_m\frac{\partial N}{\partial r} &= h_n\left(N_f - N\right), \quad \text{at } r = R,\\
w \longrightarrow w_e &= \frac{U_\infty z}{l},\\
\frac{\partial w}{\partial r} &\longrightarrow 0,\\
T &\longrightarrow T_f,\\
C &\longrightarrow C_f,\\
N &\longrightarrow N_f, \quad \text{as } r \longrightarrow \infty.
\end{aligned}
\tag{6}
$$

The following similarities are introduced for obtaining dimension system of the current problem:

$$
\begin{aligned}
u &= -\frac{R}{r}\sqrt{\frac{U_0 \nu}{l}} f(\zeta),\\
w &= \frac{U_0 z}{l} f'(\zeta),\\
\theta(\zeta) &= \frac{T - T_\infty}{T_f - T_\infty},\\
\phi(\zeta) &= \frac{C - C_\infty}{C_f - C_\infty},\\
\phi(\zeta) &= \frac{N - N_\infty}{N_f - N_\infty},\\
\zeta &= \sqrt{\frac{U_0}{\nu l}}\left(\frac{r^2 - R^2}{2R}\right),
\end{aligned}
\tag{7}
$$

$$
\begin{aligned}
&(1+2\lambda\zeta)^2\gamma_1\left[2ff'f'' - f^2 f'''\right] - (1+2\lambda\zeta)\lambda\gamma_1 f^2 f''\\
&- (1+2\lambda\zeta)^2\gamma_2\left[3f^2(f'')^2 + 2f(f')^2 f'' - f^3 f^{iv}\right]\\
&- 4\lambda^2\gamma_2 f''' f'' + (1+2\lambda\zeta)\gamma_2\left[3f^2 f' f'' + f^3 f'''\right]\\
&+ (1+2\lambda\zeta)^3\gamma_3\left[(f'')^2 - ff^{iv}\right] - 4\lambda\gamma_3(1+2\lambda\zeta)^2 ff'''\\
&+ (1+2\lambda\zeta)^3 f''' + (1+2\lambda\zeta)^2\left[2f'' + ff'' - (f')^2\right]\\
&+ (1+2\lambda\zeta)^2 A^2 - (1+2\lambda\zeta)^2 M^2\\
&\cdot\left[-A + \gamma_2 ff''' - \gamma_1 ff'' + f'\right]\\
&+ S(\theta - \mathrm{Nr}\phi - \mathrm{Nc}\chi)\sin\frac{\delta}{2} = 0,
\end{aligned}
\tag{8}
$$

$$
\begin{aligned}
&\left[\left\{Rd\left(1+\theta(\theta_w - 1)\right)^3\right\}\theta''(1+2\lambda\zeta)\right]'\\
&+ \epsilon_1\theta\theta'' + \epsilon_1\theta'^2 + \mathrm{Pr}\theta'\lambda f\\
&+ \mathrm{PrNb}\phi'\theta'(1+2\lambda\zeta) + \mathrm{PrNt}\theta'^2(1+2\lambda\zeta) = 0,
\end{aligned}
\tag{9}
$$

$$
\begin{aligned}
&[(1+2\lambda\zeta) + \epsilon_2\phi]\phi'' + \epsilon_2\phi'^2 + 2\alpha\phi' + \mathrm{LePr} f\phi'\\
&+ (1+2\lambda\zeta)\left(\frac{\mathrm{Nt}}{\mathrm{Nb}}\right)\theta'' + 2\lambda\left(\frac{\mathrm{Nt}}{\mathrm{Nb}}\right)\theta' - \mathrm{PrLe}\sigma^*\\
&\cdot(1+\delta\theta)^n \exp\left(\frac{-E}{(1+\delta\theta)}\right)\phi = 0,
\end{aligned}
\tag{10}
$$

$$
(1+2\lambda\zeta)\chi'' + 2\lambda\chi' + \mathrm{Lb} f\chi' - \mathrm{Pe}\left[\phi''(\chi+\delta_1) + \chi'\phi'\right] = 0,
\tag{11}
$$

$$\begin{aligned}
f &= 0,\\
f' &= 1,\\
\theta' &= -\alpha_1 (1-\theta(\zeta)),\\
\phi' &= -\alpha_2 (1-\phi(\zeta)),\\
\chi' &= -\alpha_3 (1-\chi(\zeta)), \quad \text{at}\ \zeta = 0,\\
f' &\longrightarrow A,\\
f'' &\longrightarrow 0,\\
\theta &\longrightarrow 0,\\
\phi &\longrightarrow 0,\\
\chi &\longrightarrow 0, \quad \text{as}\ \zeta \longrightarrow \infty.
\end{aligned} \tag{12}$$

We have that velocity ratio parameter is $A = (U_\infty/U_0)$, U_∞ denotes the velocity of free stream, U_0 stands for stretching velocity, S denotes mixed convection parameter, Nr stands for buoyancy ratio parameter, Nc stands for bioconvection Rayleigh number, α is the curvature parameter, γ_1 and γ_3 are Deborah numbers, Burgers fluid parameter is represented by γ_2, M is the magnetic parameter, Pr denotes Prandtl number, Lewis number is denoted by Le, Rd is radiation parameter, θ_w denotes temperature ratio parameter, thermophoresis parameter is Nt, Brownian motion parameter is expressed as Nb, σ^* is the reaction parameter, δ is temperature difference parameter, E represents activation energy, bioconvection Lewis number is denoted by Lb, Pe is Peclet number, microorganisms difference parameter is δ, α_1 is the thermal Biot number, α_2 is the concentration Biot number, and α_3 denotes the microorganisms Biot number, which are given as follows:

$$\begin{aligned}
S &= \frac{l^2\beta^{**} g^* (1-C_\infty)\left(T_f - T_0\right)}{zU_0^2\rho_f},\\
\mathrm{Nr} &= \frac{\left(\rho_p-\rho_f\right)\left(C_f-C_o\right)}{(1-C_\infty)\left(T_f-T_0\right)},\\
\mathrm{Nc} &= \frac{\gamma^*\left(\rho_m-\rho_f\right)\left(N_f-N_0\right)}{(1-C_\infty)\left(T_f-T_0\right)\beta^{**}},\\
\lambda &= \frac{1}{R}\sqrt{\frac{\nu l}{U_0}},\\
\gamma_1 &= \beta_1\frac{U_0}{l},\\
\gamma_3 &= \beta_3\left(\frac{U_0}{l}\right),\\
\gamma_2 &= \beta_2\left(\frac{U_0}{l}\right)^2 M = \left(\frac{\sigma l B_0^2}{\rho_f U_0}\right)^{(1/2)},\\
\mathrm{Le} &= \frac{\alpha_1}{D_B},\\
\mathrm{Pr} &= \frac{\nu}{\alpha_1},\\
\theta_w &= \frac{T_f}{T_\infty},\\
\mathrm{Rd} &= \frac{16\sigma T_\infty^3}{3kk^*},\\
\mathrm{Nt} &= \frac{\tau D_T\left(T_f-T_\infty\right)}{\nu T_\infty},\\
\mathrm{Nb} &= \frac{\tau D_B\left(C_f-C_\infty\right)}{\nu},\\
\sigma^* &= \frac{lKr^2}{U_0},\\
\delta &= \frac{T_f-T_0}{T_\infty},\\
E &= \frac{E_a}{kT},\\
\mathrm{Lb} &= \frac{\nu}{D_m},\\
\mathrm{Pe} &= \frac{bW_c}{D_m},\\
\delta_1 &= \frac{N_\infty}{N_f-N_0},\\
\alpha_1 &= \frac{h_f}{k}\sqrt{\frac{\nu l}{U_0}},\\
\alpha_2 &= \frac{h_g}{D_B}\sqrt{\frac{\nu l}{U_0}},\\
\alpha_3 &= \frac{h_n}{D_m}\sqrt{\frac{\nu l}{U_0}}.
\end{aligned} \tag{13}$$

The physical quantities of interest are defined as follows:

$$\begin{aligned}
\mathrm{Nu}_z &= \frac{zq_m}{k(T_w-T_\infty)},\\
\mathrm{Sh}_z &= \frac{zj_m}{D_B(C_w-C_\infty)},\\
\mathrm{Sn}_z &= \frac{zq_m}{D_m(N_w-N_\infty)},\\
q_m &= -k\left(\frac{\partial T}{\partial r}\right)_{r=R} - \frac{16\sigma T^3}{3k^*}\left(\frac{\partial T}{\partial r}\right)_{r=R},\\
j_m &= -D_B\left(\frac{\partial C}{\partial r}\right)_{r=R},\\
q_m &= -D_m\left(\frac{\partial N}{\partial r}\right)_{r=R},\\
\mathrm{Nu}_z\mathrm{Re}^{-(1/2)} &= -\left(1+\frac{4}{3}\left(R_d\left(1+(\theta_w-1)\theta(0)\right)\right)\right)^3\theta'(0),\\
Sh_z\mathrm{Re}^{-(1/2)} &= -\phi'(0),\\
Sn_z\mathrm{Re}^{-(1/2)} &= -\chi'(0).
\end{aligned} \tag{14}$$

3. Numerical Scheme

The numerical limitations of the dimensionless flow system (8)–(11), along with boundary restriction (12), are tackled numerically. As established equations are highly nonlinear, it is difficult to get an accurate solution. Therefore, we use a famous numerical scheme through bvp4c via MATLAB computational software. So, we have to renovate the higher-order BVP to 1st-order IVP.

Let

$$
\begin{aligned}
f &= h_1,\\
f' &= h_2,\\
f'' &= h_3,\\
f''' &= h_4,\\
f^{iv} &= h_4',\\
\theta &= h_5,\\
\theta' &= h_6,\\
\theta'' &= h_6',\\
\phi &= h_7,\\
\phi' &= h_8,\\
\phi'' &= h_8',\\
\chi &= h_9,\\
\chi' &= h_{10},\\
\chi'' &= h_{10}',\\
h_4' &= (1+2\lambda\zeta)^2\gamma_1\left[2h_1h_2h_3 - h_1^2h_4\right] - (1+2\lambda\zeta)\lambda\gamma_1 h_1^2 h_3 -\\
&\quad \cdot (1+2\lambda\zeta)^2\gamma_2\left[3h_1^2(h_3)^2 + 2h_1(h_2)^2h_3\right] - 4\lambda^2\gamma_2 h_4 h_3\\
&\quad + (1+2\lambda\zeta)\lambda\gamma_2\left[3h_1^2h_2h_3 + h_1^3h_4\right] + (1+2\lambda\zeta)^3\gamma_3(h_3)^2\\
&\quad - 4\lambda\gamma_3(1+2\lambda\zeta)^2h_1h_4 + (1+2\lambda\zeta)^3h_4 + (1+2\lambda\zeta)^2\left[2\lambda h_3 + h_1h_3 - (h_2)^2\right]\\
&\quad \frac{+(1+2\lambda\zeta)^2A^2 - (1+2\lambda\zeta)^2M^2\left[-A + \gamma_2h_1h_4 - \gamma_1h_1h_3 + h_2\right] - S\left(h_5 - \mathrm{Nr}h_7 - \mathrm{Nc}h_9\right)\sin(\delta/2)}{\left((1+2\lambda\zeta)^3\gamma_3h_1 - (1+2\lambda\zeta)^2\gamma_2h_1^3\right)}\\
h_6' &= \frac{-\mathrm{Pr}h_6h_1 - \epsilon_1h_6^2 - \mathrm{PrNb}h_8h_6(1+2\lambda\zeta) - \mathrm{PrNt}h_6^2(1+2\lambda\zeta)}{\left[\left\{\mathrm{Rd}\left(1+h_5(\theta_w-1)\right)^3\right\}(1+2\lambda\zeta) + \epsilon_1h_5\right]'},\\
&\quad -2\lambda h_8 - \mathrm{LePr}h_1h_8 - (1+2\lambda\zeta)(\mathrm{Nt}/\mathrm{Nb})h_6' - 2\lambda(\mathrm{Nt}/\mathrm{Nb})h_6\\
h_8' &= \frac{+\mathrm{PrLe}\sigma^*(1+\delta h_5)^n\exp\left(-E/(1+\delta h_5)\right)h_7 - \epsilon_2h_8^2}{\left[(1+2\lambda\zeta) + \epsilon_2h_7\right]},
\end{aligned}
$$

$$
\begin{aligned}
h_{10}' &= \frac{-2\lambda h_{10} - \mathrm{Lb} h_1 h_{10} + \mathrm{Pe}\left[h_8'\left(h_9 + \delta_1\right) + h_{10} h_8\right]}{(1 + 2\lambda\zeta)} \\
h_1 &= 0, \\
h_2 &= 1, \\
h_6 &= -\alpha_1\left(1 - h_5(\zeta)\right), \\
h_8 &= -\alpha_2\left(1 - h_7(\zeta)\right), \\
h_{10} &= -\alpha_3\left(1 - h_9(\zeta)\right), \quad \text{at } \zeta \\
h_2 &\longrightarrow A, \\
h_3 &\longrightarrow 0, \\
h_5 &\longrightarrow 0, \\
h_7 &\longrightarrow 0, \\
h_9 &\longrightarrow 0, \quad \text{as } \zeta \longrightarrow \infty.
\end{aligned} \tag{15}
$$

4. Results and Discussion

Salient features of mixed convection parameter S versus the velocity of fluid f' are illuminated in Figure 2. It is viewed that the velocity field f' is enlarged for rising values of mixed convection parameter for both values ($\lambda = 0\&0.3$). Figure 3 reflects the consequence of the buoyancy ratio parameter Nr against the velocity profile f'. The buoyancy ratio parameter reduced the velocity of Burgers nanofluid f' for both values ($\lambda = 0\&0.3$). Figure 4 displays the valuation in the velocity profile f' for bioconvection Rayleigh number Nc. It is scrutinized through the figure that the mounting magnitude of bioconvection Rayleigh number decays the velocity distribution for both cases ($\lambda = 0\&0.3$). The behaviour of Burgers fluid parameter γ_2 against the velocity field f' is clarified in Figure 5. Here velocity field f' reduced as the escalating value of the Burgers fluid parameter for both values ($\lambda = 0\&0.3$). Figure 6 elucidates the effect of Deborah numbers γ_3 versus the velocity field f'. It is noticed that the velocity of fluid f' is increased by increasing values of Deborah numbers for both cases ($\lambda = 0\&0.3$). Physically Deborah numbers γ_3 depend upon retardation to time. As a result improvement in retardation times the Deborah number increase. The acceleration is induced in the flow of fluid and velocity field is boosted up. The influence of the magnetic parameter M versus the velocity field f' is explicated in Figure 7. It is to be observed that velocity of fluid f' decays by enhancing the variation in magnetic parameter for both cases ($\lambda = 0 \& 0.3$). Consequently, the Lorentz forces are introduced via a larger magnetic parameter, so the flow of fluid reduces.

Figure 8 expounded the inspiration of Deborah numbers γ_1 on the velocity of the fluid f'. It is perceived that the velocity of fluid f' diminishes by enhancement in the magnitude of Deborah numbers for both cases of plate and cylinder ($\lambda = 0 \& 0.3$). Deborah number is the ratio of relaxation to observation times; thus, relaxation time rises with increment in Deborah number, and as a result confrontation in liquid motion swells which leads to reducing the flow of fluid. Prominent attribution of temperature ratio parameter θ_w versus temperature distribution θ is shown in Figure 9. The temperature field θ is enlarged for a larger magnitude of fluid temperature ratio parameter θ_w for both plate and cylinder ($\lambda = 0 \& 0.3$). The temperature ratio parameter improves the thermal state of liquid; therefore, the temperature field is improved. Figure 10 is deliberating the outcome of thermophoresis parameter Nt for the temperature concentration profile θ. It is pragmatic that augmentation in Nt boosted the temperature profile θ for both values ($\lambda = 0 \& 0.3$). Figure 11 shows the variations in temperature profile θ for swelling values of the Prandtl number Pr. It is regarded through drafts that the growing variations of Prandtl number Pr fall off the temperature field θ for both cases ($\lambda = 0 \& 0.3$). Physically the escalating value of Prandtl number causes a reduction in thermal diffusivity. Hence, the temperature field falls. Figure 12 is apprehended to examine the behaviour of thermal conductivity ε_1 against temperature distribution θ. It is detected that the swelling variation of the thermal conductivity causes an upsurge in the temperature field θ. The impact of thermal stratification Biot number α_1 against temperature distribution θ is accomplished in Figure 13. From the figure, it is initiated that the enhancing values of thermal stratification Biot number improved the temperature distribution for both plate and cylinder ($\lambda = 0 \& 0.3$).

Figure 14 illuminates the significance of the Prandtl number Pr for the concentration field ϕ. The increasing valuation of the Prandtl number reduces the concentration field ϕ. Figure 15 is captured to perceive the nature of thermophoresis parameter Nt against the volumetric concentration field ϕ. The approximation in the thermophoresis parameter results in a boost in the volumetric concentration of nanoparticles ϕ. Physically the solid particles transfer from hot section to cold region due to developed

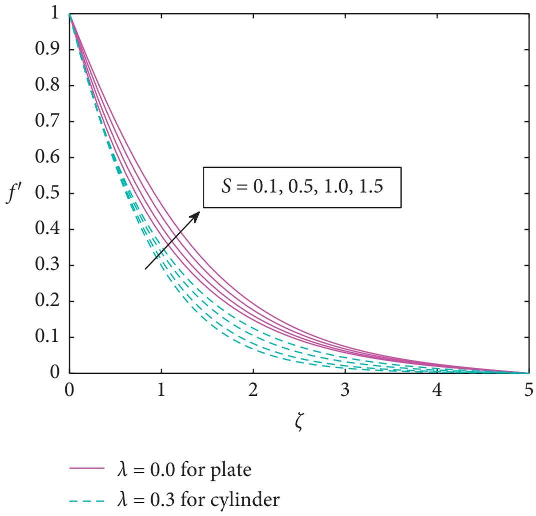

Figure 2: Disparity of S via f'.

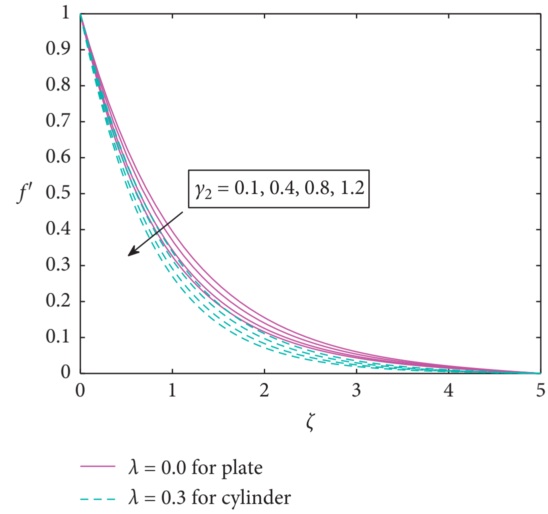

Figure 5: Disparity of γ_2 via f'.

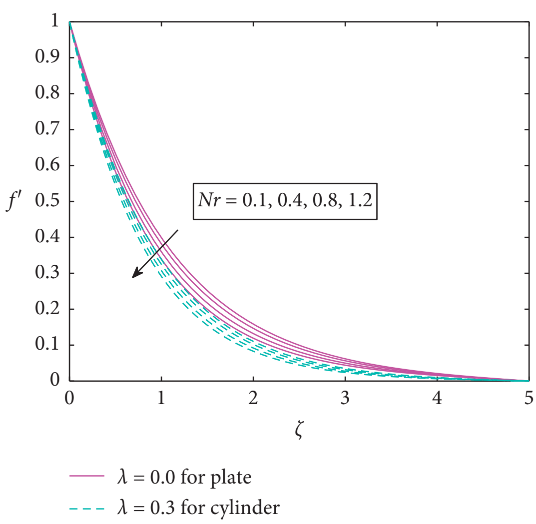

Figure 3: Disparity of Nr via f'.

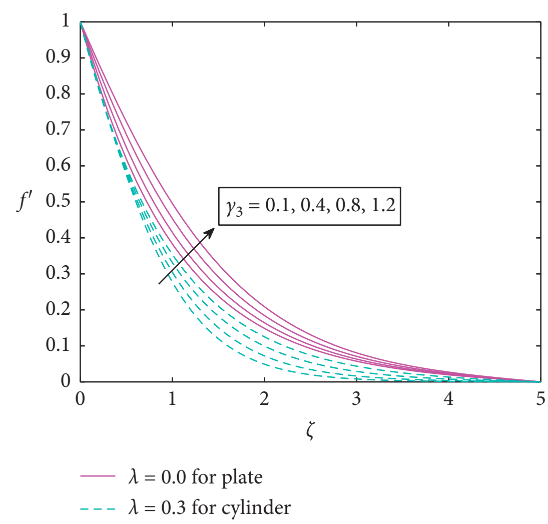

Figure 6: Disparity of γ_3 via f'.

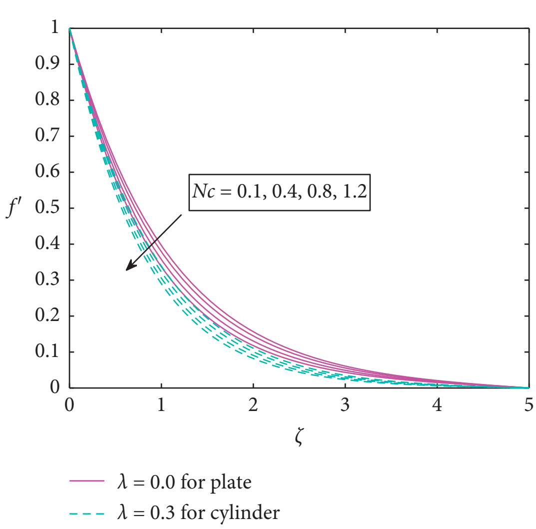

Figure 4: Disparity of Nc via f'.

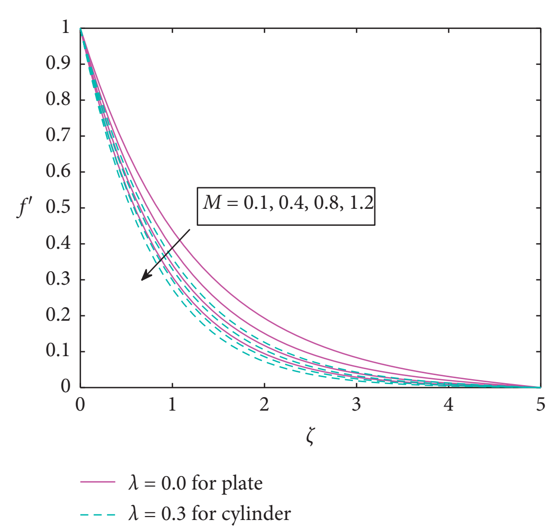

Figure 7: Disparity of M via f'.

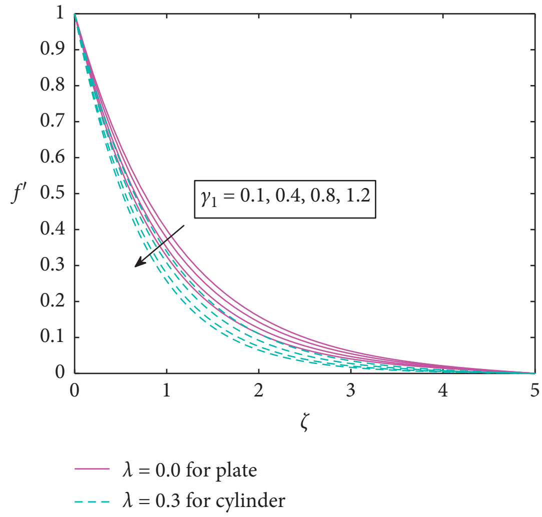

Figure 8: Disparity of γ_1 via f'.

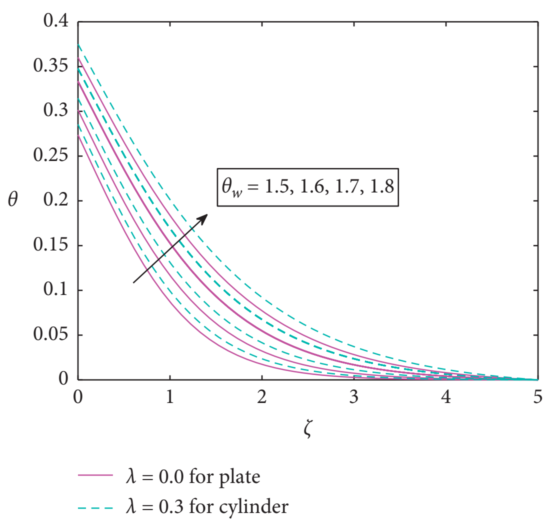

Figure 9: Disparity of θ_w via θ.

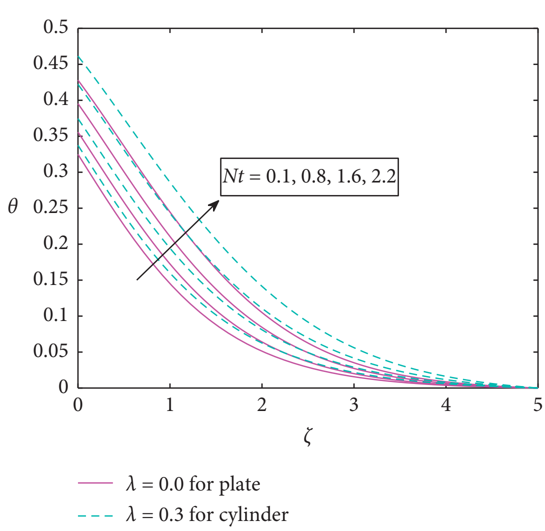

Figure 10: Disparity of Nt via θ.

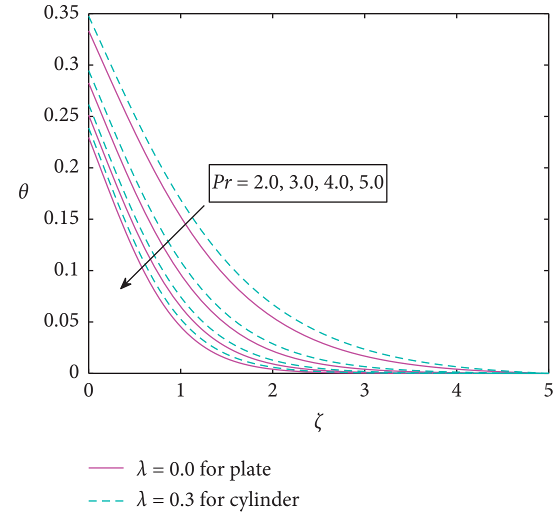

Figure 11: Disparity of Pr via θ.

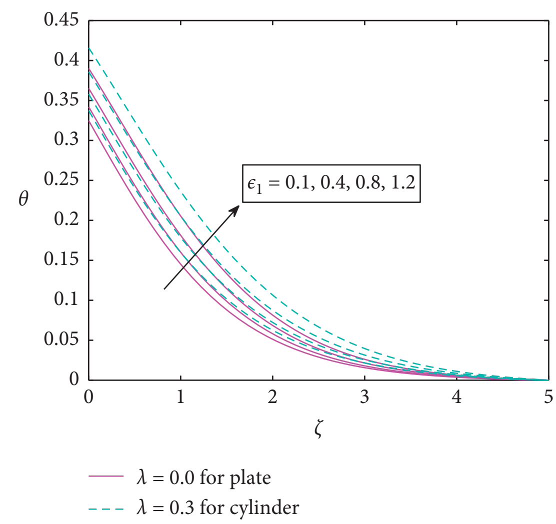

Figure 12: Disparity of ϵ_1 via θ.

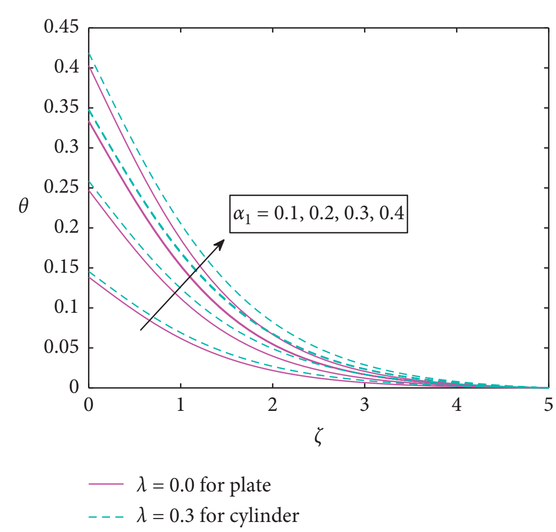

Figure 13: Disparity of α_1 via θ.

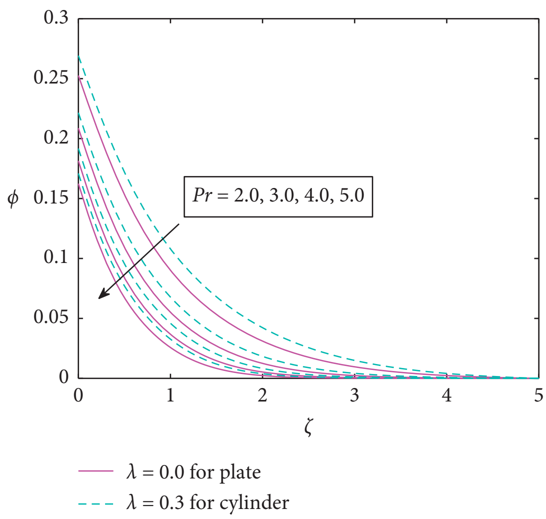

Figure 14: Disparity of Pr via ϕ.

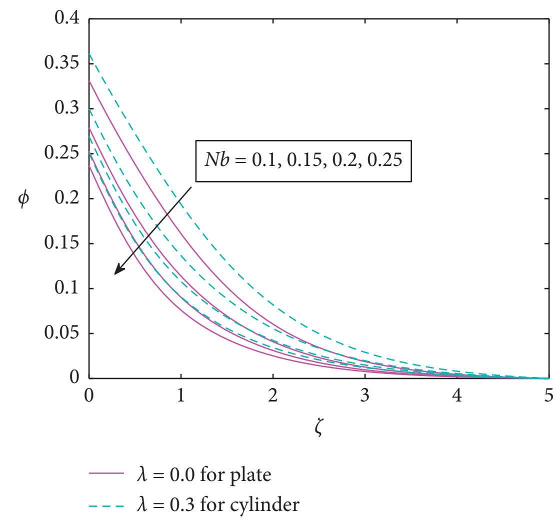

Figure 16: Disparity of Nb via ϕ.

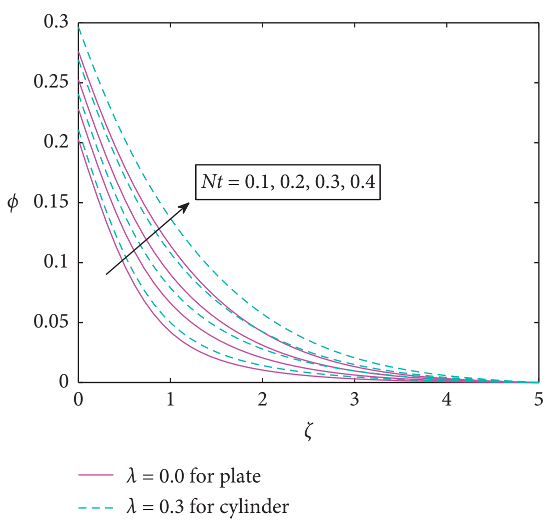

Figure 15: Disparity of Nt via ϕ.

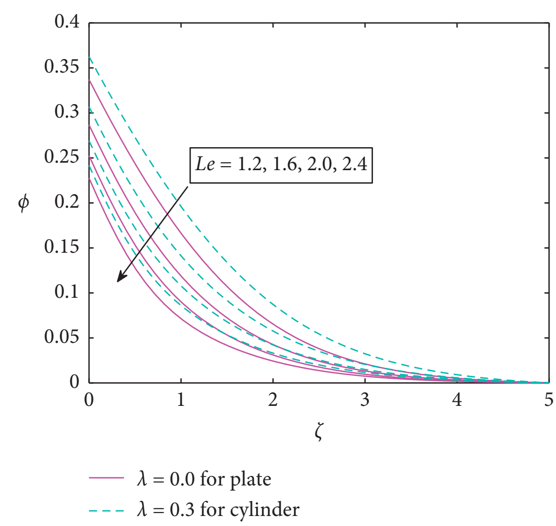

Figure 17: Disparity of Le via ϕ.

thermophoresis valuation. Outstanding features of the Brownian motion parameter Nb for the concentration field ϕ are sketched in Figure 16. Concentration field ϕ dwindles by raise in the magnitude of the Brownian motion parameter for both values $(\lambda = 0\,\&\,0.3)$. Physically Brownian motion controls the diffusion of the solid particles in the system away from the boundary. Hence, improvement of Brownian motion parameter results in a decline of concentration field. Figure 17 explicates the consequences of Lewis number Le for the concentration field of nanoparticles ϕ. By the escalation of Lewis number Le, the concentration field ϕ diminishes. Figure 18 illuminates the significance of solutal conductivity ε_2 against the concentration field ϕ of nanoparticles. It proposed that the concentration field of nanoparticles increased by the positive valuation of solutal conductivity for both values $(\lambda = 0\,\&\,0.3)$. Figure 19 describes the consequence of activation energy E versus the concentration profile of nanoparticles ϕ. It is anticipated that the concentration field of nanoparticles is amplified by the growing values of activation energy for both cases $(\lambda = 0\,\&\,0.3)$. The upshot of solutal Biot number α_2 on the concentration field ϕ of nanomaterials is portrayed in Figure 20. It is estimated that the enhancing values of activation energy augmented the concentration field of nanoparticles for both cases $(\lambda = 0\,\&\,0.3)$. Figure 21 finds the outcome of Peclet number Pe against microorganism's concentration field χ. It can be scrutinized that the microorganism's field χ declined for higher variations of Peclet number Pe. The result of the microorganism stratification Biot number α_3 against microorganism's concentration field χ is sketched in Figure 22. The microorganism's field χ is heightened for advanced values of microorganism stratification Biot number for both values $(\lambda = 0\,\&\,0.3)$. Figure 23 designates the conclusion of bioconvection Lewis number Lb against microorganism's concentration field χ. It is inspected that the microorganism's field χ is deteriorated for higher

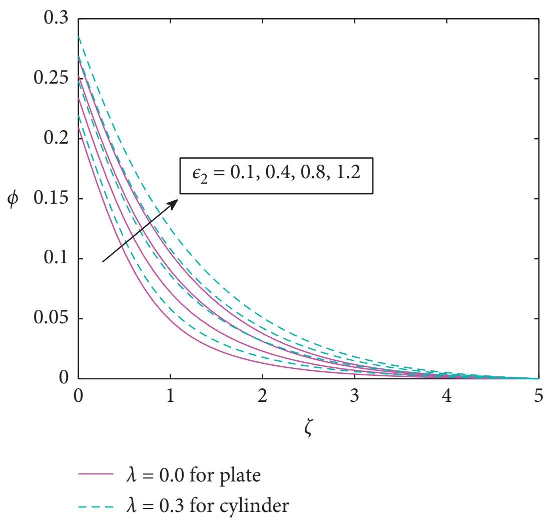

FIGURE 18: Disparity of ε_2 via ϕ.

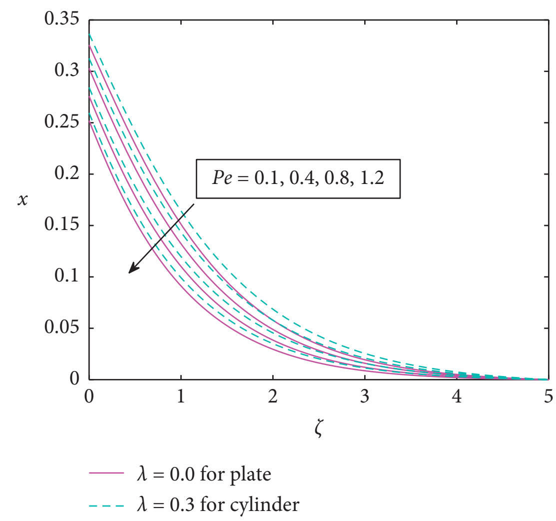

FIGURE 21: Disparity of Pe via χ.

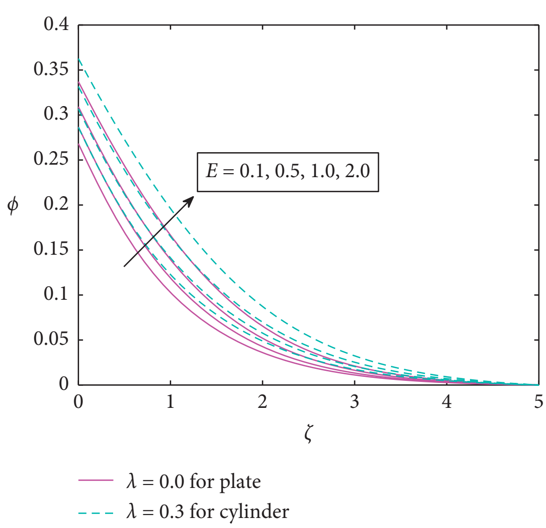

FIGURE 19: Disparity of E via ϕ.

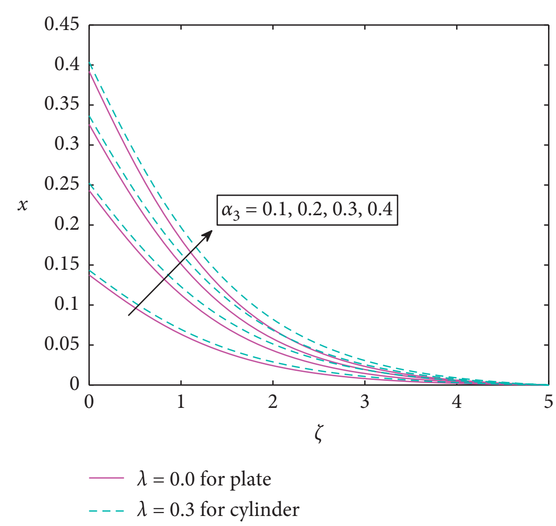

FIGURE 22: Disparity of α_3 via χ.

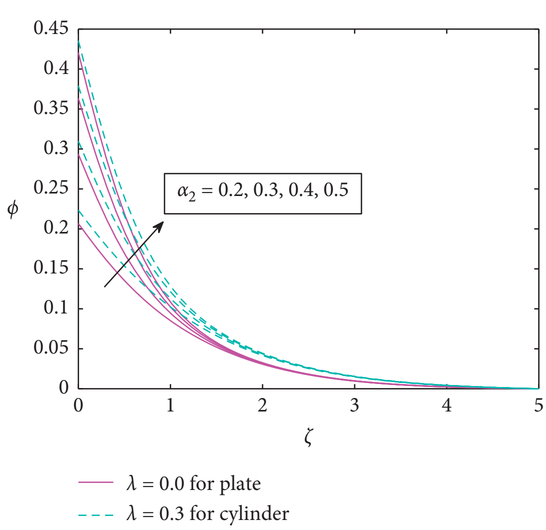

FIGURE 20: Disparity of α_2 via ϕ.

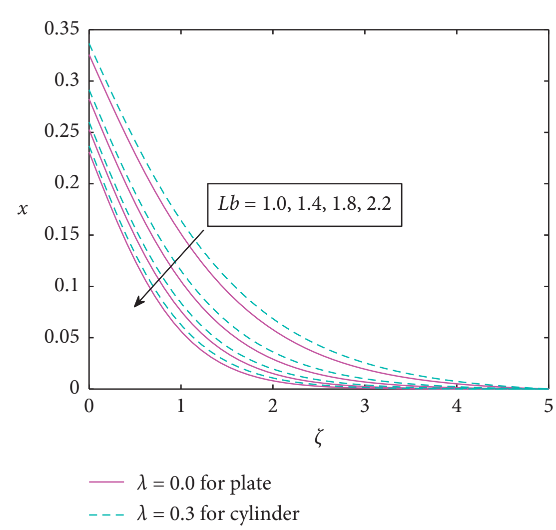

FIGURE 23: Disparity of Lb via χ.

Table 1: Comparison table for variation of $-f''(0)$ for distinct values of M in special case when $\mathrm{Nt} = \mathrm{Nb} = \mathrm{Pe} = \mathrm{Lb} = \lambda = 0$.

M	Shehzad et al. [49]	Hayat et al. [50]	Khan et al. [51]	Present study
0.0	1.00000	1.00000	1.00000	1.00000
0.2	1.01980	1.01980	1.019801	1.019807
0.5	1.11803	1.11803	1.118029	1.118030
0.8	1.28063	1.28063	1.280633	1.280634
1.0	1.41421	1.41421	1.414221	1.414222
1.2	1.56205	1.56205	1.562048	1.562048
1.5	1.80303	1.80303	1.803044	1.803045

Table 2: Numerical result of local skin friction $-f''(0)$ Versus M, S, Nr, Nc, γ_3, γ_1, and γ_2.

Parameters							$-f''(0)$	
M	S	Nr	Nc	γ_3	γ_1	γ_2	$\lambda = 0.0$	$\lambda = 0.3$
0.1							**0.8241**	**0.9838**
0.6	0.2	0.1	0.1	0.3	0.1	1.0	**0.9643**	**1.0833**
1.2							**1.0966**	**1.1837**
	0.1						**0.8414**	**0.8518**
0.5	**1.0**	0.1	0.1	0.3	0.1	1.0	**0.9772**	**1.3168**
	2.0						**1.1015**	**1.4637**
		0.2					**0.8493**	**0.8561**
0.5	0.2	**1.0**	0.1	0.3	0.1	1.0	**1.3127**	**1.4061**
		2.0					**1.6714**	**1.7179**
			0.2				**0.8384**	**0. 8690**
0.5	0.2	0.1	**1.0**	0.3	0.1	1.0	**1.0143**	**0.9821**
			2.0				**1.0244**	**1.2969**
				0.1			**0.9584**	**1.0853**
0.5	0.2	0.1	0.1	**0.6**	0.1	1.0	**0.9104**	**0.9829**
				1.2			**0.8548**	**0.9739**
					0.1		**0.9101**	**1.0339**
0.5	0.2	0.1	0.1	0.3	**0.6**	1.0	**1.0093**	**1.1249**
					1.2		**1.1151**	**1.2150**
						0.1	**0.9172**	**1.0407**
0.5	0.2	0.1	0.1	0.3	0.1	**0.6**	**0.9731**	**1.2115**
						1.2	**1.0452**	**1.3665**

Table 3: Numerical results of $-\theta'(0)$ corresponding to M, S, Nc, Nr, Nt, NbPr, Rd, λ_1, and Le.

M	S	Nc	Nr	Nt	Nb	Pr	Rd	α_1	Le	$-\theta'(0)$	
										$\lambda = 0.0$	$\lambda = 0.3$
0.1										**0.1827**	**0.1772**
0.6	0.2	0.1	0.1	0.3	0.2	1.2	0.8	0.3	2.0	**0.1788**	**0.1746**
1.2										**0.1754**	**0.1721**
	0.2									**0.1840**	**0.1758**
0.5	**1.6**	0.1	0.1	0.3	0.2	1.2	0.8	0.3	2.0	**0.1882**	**0.1767**
	2.0									**0.1828**	**0.1769**
		0.2								**0.1848**	**0.1759**
0.5	0.2	**1.0**	0.1	0.3	0.2	1.2	0.8	0.3	2.0	**0.1720**	**0.1655**
		2.0								**0.1683**	**0.1549**
			0.2							**0.1848**	**0.1759**
0.5	0.2	0.1	**1.0**	0.3	0.2	1.2	0.8	0.3	2.0	**0.1732**	**0.1754**
			2.0							**0.1619**	**0.1747**
				0.1						**0.1814**	**0.1767**
0.5	0.2	0.1	0.1	**0.6**	0.2	1.2	0.8	0.3	2.0	**0.1765**	**0.1707**
				1.2						**0.1703**	**0.1632**
					0.1					**0.1802**	**0.1760**
0.5	0.2	0.1	0.1	0.3	**0.6**	1.2	0.8	0.3	2.0	**0.1771**	**0.1723**
					1.2					**0.1735**	**0.1681**

Table 3: Continued.

M	S	Nc	Nr	Nt	Nb	Pr	Rd	α_1	Le	$-\theta'(0)$	
										$\lambda = 0.0$	$\lambda = 0.3$
						2.0				0.2005	0.1963
0.5	0.2	0.1	0.1	0.3	0.2	3.0	0.8	0.3	2.0	0.2158	0.2123
						4.0				0.2253	0.2223
							0.1			0.1996	0.1963
0.5	0.2	0.1	0.1	0.3	0.2	1.2	0.6	0.3	2.0	0.1843	0.1808
							1.2			0.1715	0.1795
								0.1		0.0821	0.0813
0.5	0.2	0.1	0.1	0.3	0.2	1.2	0.8	0.6	2.0	0.2529	0.2438
								1.2		0.3158	0.3013
									1.0	0.1796	0.1751
0.5	0.2	0.1	0.1	0.3	0.2	1.2	0.8	0.3	1.6	0.1795	0.1750
									2.2	0.1794	0.1749

Table 4: Numerical results of local Sherwood number $-\phi'(0)$ corresponding to M, S, Nc, Nr, Nt, Nb, Pr, γ_1, γ_2, Le, and α_2.

M	S	Nc	Nr	Nt	Nb	Pr	γ_1	γ_2	Le	α_2	$-\phi'(0)$	
											$\lambda = 0.0$	$\lambda = 0.3$
0.1											0.1494	0.1450
0.6	0.2	0.1	0.1	0.3	0.2	1.2	0.3	0.3	2.0	0.3	0.1474	0.1439
1.2											0.1430	0.1428
	0.2										0.1482	0.1476
0.5	1.6	0.1	0.1	0.3	0.2	1.2	0.3	0.3	2.0	0.3	0.1460	0.1458
	2.0										0.1424	0.1419
		0.2									0.1486	0.1468
0.5	0.2	1.0	0.1	0.3	0.2	1.2	0.3	0.3	2.0	0.3	0.1452	0.1449
		2.0									0.1438	0.1425
			0.2								0.1479	0.1469
0.5	0.2	0.1	1.0	0.3	0.2	1.2	0.3	0.3	2.0	0.3	0.1460	0.1451
			2.0								0.1451	0.1446
				0.1							0.1610	0.1616
0.5	0.2	0.1	0.1	0.6	0.2	1.2	0.3	0.3	2.0	0.3	0.1301	0.1384
				1.2							0.1229	0.1168
					0.1						0.1281	0.1209
0.5	0.2	0.1	0.1	0.3	0.6	1.2	0.3	0.3	2.0	0.3	0.1614	0.1596
					1.2						0.1647	0.1684
						2.0					0.1587	0.1553
0.5	0.2	0.1	0.1	0.3	0.2	3.0	0.3	0.3	2.0	0.3	0.1662	0.1636
						4.0					0.1708	0.1687
							0.1				0.1488	0.1443
0.5	0.2	0.1	0.1	0.3	0.2	1.2	0.8	0.3	2.0	0.3	0.1476	0.1434
							1.6				0.1461	0.1424
								0.1			0.1483	0.1444
0.5	0.2	0.1	0.1	0.3	0.2	1.2	0.3	0.8	2.0	0.3	0.1476	0.1433
								1.6			0.1461	0.1422
									1.0		0.1221	0.1158
0.5	0.2	0.1	0.1	0.3	0.2	1.2	0.3	0.3	1.6	0.3	0.1406	0.1358
									2.2		0.1510	0.1473
										0.1	0.0804	0.0788
0.5	0.2	0.1	0.1	0.3	0.2	1.2	0.3	0.3	2.0	0.6	0.2368	0.2309
										1.2	0.4945	0.4899

values of bioconvection Lewis number for both plate and cylinder ($\lambda = 0.0\,\&\,0.3$).

The numerical outcomes of the skin friction coefficient, local Nusselt number, local Sherwood number, and local density number of motile microorganisms against developed parameters are captured through Tables 1–5. In Table 1, we accomplished the comparison. From Table 2, the local skin friction coefficient succeeds with M while reducing for S. In

Table 5: The numerical results of $-\chi'(0)$ for M, S, Nr, Nc, γ_3, Pe, Lb, and α_3.

Parameters								$-\chi'(0)$	
M	S	Nr	Nc	γ_3	Pe	Lb	α_3	$\lambda = 0.0$	$\lambda = 0.3$
0.1								**0.2036**	**0.1997**
0.6	0.2	0.1	0.1	0.3	0.1	1.0	0.3	**0.2001**	**0.1975**
1.2								**0.1977**	**0.1953**
	0.1							**0.2014**	**0.1918**
0.5	**1.0**	0.1	0.1	0.3	0.1	1.0	0.3	**0.1927**	**0.1848**
	2.0							**0.1815**	**0.1837**
		0.2						**0.2039**	**0.1930**
0.5	0.2	**1.0**	0.1	0.3	0.1	1.0	0.3	**0.2027**	**0.1916**
		2.0						**0.2013**	**0.1997**
			0.2					**0.2048**	**0.2929**
0.5	0.2	0.1	**1.0**	0.3	0.1	1.0	0.3	**0.2043**	**0.1812**
			2.0					**0.2034**	**0.1889**
				0.1				**0.2009**	**0.1975**
0.5	0.2	0.1	0.1	**0.6**	0.1	1.0	0.3	**0.2015**	**0.1952**
				1.2				**0.2023**	**0.1931**
					0.2			**0.2027**	**0.1994**
0.5	0.2	0.1	0.1	0.3	**1.0**	1.0	0.3	**0.2137**	**0.2109**
					2.0			**0.2252**	**0.2227**
						1.2		**0.2084**	**0.2055**
0.5	0.2	0.1	0.1	0.3	0.1	**2.0**	0.3	**0.2271**	**0.2251**
						3.0		**0.2395**	**0.2382**
							0.1	**0.0860**	**0.0817**
0.5	0.2	0.1	0.1	0.3	0.1	1.0	**0.6**	**0.3032**	**0.2993**
							1.2	**0.4047**	

Table 3, it can be noticed that the local Nusselt number turns down for a larger amount Rd. From Table 4, it is scrutinized that the local Sherwood number boosted up with various values of α_2. The rescaled density number of motile microorganisms is diminishing function of γ_3, which is shown in Table 5.

As a significance, from these tables, we are assured that the recent results are very accurate.

5. Concluding Remarks

The thermal and solutal conductivity phenomena for magneto-Burgers nanofluid with swimming motile microorganisms were established. The eminent shooting method is employed to crack the flow problems of magneto-Burgers nanofluid via bvp4c solver in computational software MATLAB. The main outcomes are highlighted as follows:

(i) It is scrutinized that the velocity of magneto-Burgers nanofluid signifies reducing trend for higher buoyancy ratio parameter, Burgers fluid parameter, and bioconvection Rayleigh number.

(ii) An improvement in the mixed convection parameter and Deborah numbers enhances velocity field.

(iii) Temperature distribution declines with a larger Prandtl number, while an inverse trend is shown for thermal Biot number.

(iv) An increment in the variations of solutal conductivity and activation energy enhances the volumetric concentration of nanoparticles.

(v) The rescaled microorganism's field exaggerates with microorganisms Biot number while it dwindles for Peclet number and bioconvection Lewis number.

Data Availability

The data that support the findings of this study are available from the corresponding author upon reasonable request.

Conflicts of Interest

The authors declare that they have no conflicts of interest.

References

[1] S. U. Choi and J. A. Eastman, "Enhancing thermal conductivity of fluids with nanoparticles," *Argonne National Lab*, vol. 1Lemont, IL, USA, 1995.

[2] J. Buongiorno, "Convective transport in nanofluids," *Journal of Heat Transfer*, vol. 128, no. 3, pp. 240–250, 2006.

[3] G. Huminic and A. Huminic, "Entropy generation of nanofluid and hybrid nanofluid flow in thermal systems: a review," *Journal of Molecular Liquids*, vol. 302, Article ID 112533, 2020.

[4] T. Hayat, S. Qayyum, A. Alsaedi, and B. Ahmad, "Entropy generation minimization: Darcy-Forchheimer nanofluid flow due to curved stretching sheet with partial slip," *International Communications in Heat and Mass Transfer*, vol. 111, Article ID 104445, 2020.
[5] R. Ellahi, F. Hussain, S. Asad Abbas, M. M. Sarafraz, M. Goodarzi, and M. S. Shadloo, "Study of two-phase Newtonian nanofluid flow hybrid with Hafnium particles under the effects of slip," *Inventions*, vol. 5, no. 1, p. 6, 2020.
[6] I. Waini, A. Ishak, T. Groşan, and I. Pop, "Mixed convection of a hybrid nanofluid flow along a vertical surface embedded in a porous medium," *International Communications in Heat and Mass Transfer*, vol. 114, Article ID 104565, 2020.
[7] A. Alsaedi, T. Hayat, S. Qayyum, and R. Yaqoob, "Eyring-Powell nanofluid flow with nonlinear mixed convection: entropy generation minimization," *Computer Methods and Programs in Biomedicine*, vol. 186, Article ID 105183, 2020.
[8] S. Lahmar, M. Kezzar, M. R. Eid, and M. R. Sari, "Heat transfer of squeezing unsteady nanofluid flow under the effects of an inclined magnetic field and variable thermal conductivity," *Physica A: Statistical Mechanics and Its Applications*, vol. 540, Article ID 123138, 2020.
[9] L. Yang, J.-N. Huang, M. Mao, and W. Ji, "Numerical assessment of Ag-water nano-fluid flow in two new microchannel heatsinks: thermal performance and thermodynamic considerations," *International Communications in Heat and Mass Transfer*, vol. 110, Article ID 104415, 2020.
[10] N. C. Roşca, A. V. Roşca, I. Pop, and J. H. Merkin, "Nanofluid flow by a permeable stretching/shrinking cylinder," *Heat and Mass Transfer*, vol. 56, no. 2, pp. 547–557, 2020.
[11] W. A. Khan, M. Waqas, W. Chammam, Z. Asghar, U. A. Nisar, and S. Z. Abbas, "Evaluating the characteristics of magnetic dipole for shear-thinning Williamson nanofluid with thermal radiation," *Computer Methods and Programs in Biomedicine*, vol. 191, Article ID 105396, 2020.
[12] A. Wu, S. Z. Abbas, Z. Asghar, H. Sun, M. Waqas, and W. A. Khan, "A shear-rate-dependent flow generated via the magnetically controlled metachronal motion of artificial cilia," *Biomechanics and Modeling in Mechanobiology*, vol. 19, pp. 1–12, 2020.
[13] S. Z. Abbas, M. I. Khan, S. Kadry, W. A. Khan, M. Israr-Ur-Rehman, and M. Waqas, "Fully developed entropy optimized second order velocity slip MHD nanofluid flow with activation energy," *Computer Methods and Programs in Biomedicine*, vol. 190, Article ID 105362, 2020.
[14] S. Z. Abbas, W. A. Khan, S. Kadry, M. I. Khan, M. Waqas, and M. I. Khan, "Entropy optimized Darcy-Forchheimer nanofluid (Silicon dioxide, Molybdenum disulfide) subject to temperature dependent viscosity," *Computer Methods and Programs in Biomedicine*, vol. 190, Article ID 105363, 2020.
[15] S. Z. Abbas, W. A. Khan, M. M. Gulzar, T. Hayt, M. Waqas, and Z. Asghar, "Magnetic field influence in three-dimensional rotating micropolar nanoliquid with convective conditions," *Computer Methods and Programs in Biomedicine*, vol. 189, Article ID 105324, 2020.
[16] S. Z. Abbas, W. A. Khan, M. Waqas, M. Irfan, and Z. Asghar, "Exploring the features for flow of Oldroyd-B liquid film subjected to rotating disk with homogeneous/heterogeneous processes," *Computer Methods and Programs in Biomedicine*, vol. 189, Article ID 105323, 2020.
[17] S. Z. Abbas, W. A. Khan, H. Sun, M. Irfan, M. I. Khan, and M. Waqas, "Von Kármán swirling analysis for modelling Oldroyd-B nanofluid considering cubic autocatalysis," *Physica Scripta*, vol. 95, no. 1, Article ID 015206, 2019.
[18] M. Khan and W. A. Khan, "Forced convection analysis for generalized Burgers nanofluid flow over a stretching sheet," *AIP Advances*, vol. 5, no. 10, Article ID 107138, 2015.
[19] W. A. Khan, M. Khan, and R. Malik, "The three-dimensional flow of an Oldroyd-B nanofluid towards stretching surface with heat generation/absorption," *PLoS One*, vol. 9, no. 8, Article ID e105107, 2014.
[20] W. A. Khan and M. Khan, "Impact of thermophoresis particle deposition on three-dimensional radiative flow of Burgers fluid," *Results in Physics*, vol. 6, pp. 829–836, 2016.
[21] M. I. Khan, S. A. Khan, T. Hayat, S. Qayyum, and A. Alsaedi, "Entropy generation analysis in MHD flow of viscous fluid by a curved stretching surface with cubic autocatalysis chemical reaction," *The European Physical Journal Plus*, vol. 135, no. 2, pp. 1–17, 2020.
[22] M. M. Ghalib, A. A. Zafar, M. B. Riaz, Z. Hammouch, and K. Shabbir, "Analytical approach for the steady MHD conjugate viscous fluid flow in a porous medium with nonsingular fractional derivative," *Physica A: Statistical Mechanics and Its Applications*, vol. 554, Article ID 123941, 2020.
[23] M. W. A. Khan, M. I. Khan, T. Hayat, and A. Alsaedi, "Numerical solution of MHD flow of power-law fluid subject to convective boundary conditions and entropy generation," *Computer Methods and Programs in Biomedicine*, vol. 188, Article ID 105262, 2020.
[24] A. Q. Mohamad, Z. Ismail, M. Omar et al., "Exact solutions on mixed convection flow of accelerated non-coaxial rotation of MHD viscous fluid with porosity effect," in *Defect and Diffusion Forum,* vol. 399, pp. 26–37, Trans Tech Publications Ltd, 2020.
[25] T. Hayat, R. Riaz, A. Aziz, and A. Alsaedi, "Influence of Arrhenius activation energy in MHD flow of third grade nanofluid over a nonlinear stretching surface with convective heat and mass conditions," *Physica A: Statistical Mechanics and Its Applications*, vol. 549, Article ID 124006, 2020.
[26] M. T. Dinh, I. Tlili, R. N. Dara, A. Shafee, Y. Y. Y. Al-Jahmany, and T. Nguyen-Thoi, "Nanomaterial treatment due to imposing MHD flow considering melting surface heat transfer," *Physica A: Statistical Mechanics and Its Applications*, vol. 541, Article ID 123036, 2020.
[27] M.-E. M. Khedr, A. J. Chamkha, and M. Bayomi, "MHD flow of a micropolar fluid past a stretched permeable surface with heat generation or absorption," *Nonlinear Analysis: Modelling and Control*, vol. 14, no. 1, pp. 27–40, 2009.
[28] A. Zaraki, M. Ghalambaz, A. J. Chamkha, M. Ghalambaz, and D. De Rossi, "Theoretical analysis of natural convection boundary layer heat and mass transfer of nanofluids: effects of size, shape and type of nanoparticles, type of base fluid and working temperature," *Advanced Powder Technology*, vol. 26, no. 3, pp. 935–946, 2015.
[29] A. J. Chamkha, "MHD-free convection from a vertical plate embedded in a thermally stratified porous medium with Hall effects," *Applied Mathematical Modelling*, vol. 21, no. 10, pp. 603–609, 1997.
[30] A. J. Chamkha and A. R. A. Khaled, "Hydromagnetic combined heat and mass transfer by natural convection from a permeable surface embedded in a fluid-saturated porous medium," *International Journal of Numerical Methods for Heat & Fluid Flow*, vol. 10, 2000.
[31] P. S. Reddy, P. Sreedevi, and A. J. Chamkha, "MHD boundary layer flow, heat and mass transfer analysis over a rotating disk through porous medium saturated by Cu-water and Ag-water

nanofluid with chemical reaction," *Powder Technology*, vol. 307, pp. 46–55, 2017.

[32] A. J. Chamkha, "Coupled heat and mass transfer by natural convection about a truncated cone in the presence of magnetic field and radiation effects," *Numerical Heat Transfer, Part A: Applications*, vol. 39, no. 5, pp. 511–530, 2001.

[33] M. Modather and A. Chamkha, "An analytical study of MHD heat and mass transfer oscillatory flow of a micropolar fluid over a vertical permeable plate in a porous medium," *Turkish Journal of Engineering and Environmental Sciences*, vol. 33, no. 4, pp. 245–258, 2010.

[34] A. Al-Mudhaf and A. J. Chamkha, "Similarity solutions for MHD thermosolutal Marangoni convection over a flat surface in the presence of heat generation or absorption effects," *Heat and Mass Transfer*, vol. 42, no. 2, pp. 112–121, 2005.

[35] H. S. Takhar, A. J. Chamkha, and G. Nath, "Unsteady flow and heat transfer on a semi-infinite flat plate with an aligned magnetic field," *International Journal of Engineering Science*, vol. 37, no. 13, pp. 1723–1736, 1999.

[36] S. K. Mondal and D. Pal, "Mathematical analysis for Brownian motion of nonlinear thermal bioconvective stagnation point flow in a nanofluid using DTM and RKF method," *Journal of Computational Design and Engineering*, vol. 7, 2020.

[37] H. Waqas, S. U. Khan, M. M. Bhatti, and M. Imran, "Significance of bioconvection in the chemical reactive flow of magnetized Carreau–Yasuda nanofluid with thermal radiation and second-order slip," *Journal of Thermal Analysis and Calorimetry*, vol. 140, pp. 1–14, 2020.

[38] H. Waqas, S. U. Khan, S. A. Shehzad, M. Imran, and I. Tlili, "Activation energy and bioconvection aspects in generalized second-grade nanofluid over a Riga plate: a theoretical model," *Applied Nanoscience*, vol. 10, pp. 1–14, 2020.

[39] S. U. Khan, H. Waqas, M. M. Bhatti, and M. Imran, "Bioconvection in the rheology of magnetized couple stress nanofluid featuring activation energy and Wu's slip," *Journal of Non-equilibrium Thermodynamics*, vol. 45, no. 1, pp. 81–95, 2020.

[40] O. A. Beg, M. Aneja, S. A. P. N. A. Sharma, and S. Kuharat, "Computation of electro-conductive gyrotactic bioconvection from a nonlinear inclined stretching sheet under non-uniform magnetic field: simulation of smart bio-nano-polymer coatings for solar energy," *International Journal of Modern Physics B*, vol. 34, 2020.

[41] M. M. Bhatti and E. E. Michaelides, "Study of Arrhenius activation energy on the thermo-bioconvection nanofluid flow over a Riga plate," *Journal of Thermal Analysis and Calorimetry*, vol. 74, pp. 1–10, 2020.

[42] S. M. H. Zadeh, S. A. M. Mehryan, M. A. Sheremet, M. Izadi, and M. Ghodrat, "Numerical study of mixed bio-convection associated with a micropolar fluid," *Thermal Science and Engineering Progress*, vol. 18, Article ID 100539, 2020.

[43] T. Muhammad, S. Z. Alamri, H. Waqas, D. Habib, and R. Ellahi, "Bioconvection flow of magnetized Carreau nanofluid under the influence of slip over a wedge with motile microorganisms," *Journal of Thermal Analysis and Calorimetry*, 2020.

[44] Z. Abdelmalek, S. U. Khan, H. Waqas, A. Riaz, I. A. Khan, and I. Tlili, "A mathematical model for bioconvection flow of Williamson nanofluid over a stretching cylinder featuring variable thermal conductivity, activation energy and second-order slip," *Journal of Thermal Analysis and Calorimetry*, pp. 1–13, 2020.

[45] Z. Abdelmalek, S. Ullah Khan, H. Waqas, H. Nabwey, and I. Tlili, "Utilization of second order slip, activation energy and viscous dissipation consequences in thermally developed flow of third grade nanofluid with gyrotactic microorganisms," *Symmetry*, vol. 12, no. 2, p. 309, 2020.

[46] A. M. Alwatban, S. U. Khan, H. Waqas, and I. Tlili, "Interaction of Wu's slip features in bioconvection of eyring powell nanoparticles with activation energy," *Processes*, vol. 7, no. 11, p. 859, 2019.

[47] C. S. Balla, R. Alluguvelli, K. Naikoti, and O. D. Makinde, "Effect of chemical reaction on bioconvective flow in oxytactic microorganisms suspended porous cavity," *Journal of Applied and Computational Mechanics*, vol. 6, pp. 653–664, 2020.

[48] R. Naz, M. Noor, T. Hayat, M. Javed, and A. Alsaedi, "Dynamism of magnetohydrodynamic cross nanofluid with particulars of entropy generation and gyrotactic motile microorganisms," *International Communications in Heat and Mass Transfer*, vol. 110, Article ID 104431, 2020.

[49] S. A. Shehzad, T. Hayat, and A. Alsaedi, "Influence of convective heat and mass conditions in MHD flow of nanofluid," *Bulletin of the Polish Academy of Sciences Technical Sciences*, vol. 63, no. 2, pp. 465–474, 2015.

[50] T. Hayat, M. Waqas, S. A. Shehzad, and A. Alsaedi, "On model of Burgers fluid subject to magneto nanoparticles and convective conditions," *Journal of Molecular Liquids*, vol. 222, pp. 181–187, 2016.

[51] M. Khan, Z. Iqbal, and A. Ahmed, "Stagnation point flow of magnetized Burgers' nanofluid subject to thermal radiation," *Applied Nanoscience*, vol. 10, 2020.